Material Strength and Applied Mechanics
A. Khotsianovsky (Ed.)

doi:10.3233/ATDE230426

Numerical Study of the Deformations of the Vane Wheel Considering Two-Way Fluid-Structure Interaction

Jiangtao LI[a], Jian HU [b], Hongbin FU [b], and Jianxin REN [b,1]
[a] *Marine Design & Research Institute of China, Shanghai 200011, China*
[b] *College of Shipbuilding Engineering, Harbin Engineering University, Harbin, 150001, China*

Abstract. As energy saving device, the vane wheel located in the downstream of propeller recovers energy from propeller wake. The deformations on the vane wheel are studied in present study considering Two-way fluid-structure interaction. The distributions of deformation and subsequent hydrodynamic performance change are discussed in present study. Results show that the numerical method employed in present study is reliable. The blade tip of vane wheel suffers severer deformations. The structural stress is concentrate at the interface of inner part and outer part.

Keywords. Vane wheel, hydrodynamic performance, fluid-structure interaction.

Nomenclature

D	Diameter of propeller (m)	ρ	density of the fluid (kg/m^3)
J	Advance coefficient (-)	T_{VV}	vane wheel's thrust (N)
T_{VR}	propeller's thrust (N)	Q_{VV}	vane wheel's torque (N·m)
Q_{VR}	propeller's torque (N·m)	K_T	thrust coefficient of vane wheel (-)
K_{TVR}	thrust coefficient of propeller (-)	K_Q	torque coefficient of vane wheel (-)
K_{QVR}	torque coefficient of propeller (-)	η	propulsion efficiency of propeller (-)
η_{VR}	propulsion efficiency of propeller (-)		

1. Introduction

The vane wheel operating in the downstream of propeller, which can recover energy from the propeller wake. The rotation of vane wheel results in extra thrust which means higher efficiency [1-4].

Based on the above advantages, the application of vane wheel is more extensive. Kehr [5], Chen [6], Lee [7] and others proposed the design methods of vane wheel based on lift line theory and induced velocity, Seok [8] established the analysis algorithm and design program of vane wheel based on the surface element method, and Hu [9] simulated the open water performance and flow field characteristics of vane wheel based on CFD method.

[1]Corresponding Author: Jianxin REN, E-mail: 898842556@qq.com.

Based on the large eddy simulation method, a numerical simulation method considering the interaction between fluid and structure is established. Present study is carried out with commercial software STAR-CCM+.

2. Governing Equation

The expression of the conservation of mass equation is:

$$\frac{\partial \rho}{\partial t}+\frac{\partial(\rho u)}{\partial x}+\frac{\partial(\rho v)}{\partial y}+\frac{\partial(\rho w)}{\partial z}=0 \tag{1}$$

In the equation, u, v, and w are the velocity components of the fluid velocity on the x-axis, y-axis, and z-axis, respectively; ρ Is the fluid density; t is the time. Since this paper assumes that water is incompressible fluid, the above formula can be simplified:

$$\frac{\partial u}{\partial x}+\frac{\partial v}{\partial y}+\frac{\partial w}{\partial z}=0 \tag{2}$$

The expression of the momentum conservation equation in the x, y, and z directions is as follows:

$$\begin{cases}\dfrac{\partial(\rho u)}{\partial t}+div\left(\rho u\bar{u}\right)=-\dfrac{\partial p}{\partial x}+\dfrac{\partial \tau_{xx}}{\partial x}+\dfrac{\partial \tau_{yx}}{\partial y}+\dfrac{\partial \tau_{zx}}{\partial z}+F_x\\ \dfrac{\partial(\rho v)}{\partial t}+div\left(\rho v\bar{u}\right)=-\dfrac{\partial p}{\partial y}+\dfrac{\partial \tau_{xy}}{\partial x}+\dfrac{\partial \tau_{yy}}{\partial y}+\dfrac{\partial \tau_{zy}}{\partial z}+F_y\\ \dfrac{\partial(\rho w)}{\partial t}+div\left(\rho w\bar{u}\right)=-\dfrac{\partial p}{\partial z}+\dfrac{\partial \tau_{xz}}{\partial x}+\dfrac{\partial \tau_{yz}}{\partial y}+\dfrac{\partial \tau_{zz}}{\partial z}+F_z\end{cases} \tag{3}$$

In the equation, p is the pressure, F_x, F_y, F_z and represents the external volume force and gravitational volume force along the x, y, and z directions, respectively, and τ_{ij} represents the stress tensor along different directions.

For the research object of this paper, the fluid is incompressible, F_x=F_y=0, F_z=ρz, so the above formula can be simplified:

$$\begin{cases}\dfrac{\partial(\rho u)}{\partial t}+div\left(\rho u\bar{u}\right)=\dfrac{\partial \tau_{xx}}{\partial x}+\dfrac{\partial \tau_{yx}}{\partial y}+\dfrac{\partial \tau_{zx}}{\partial z}\\ \dfrac{\partial(\rho v)}{\partial t}+div\left(\rho v\bar{u}\right)=\dfrac{\partial \tau_{xy}}{\partial x}+\dfrac{\partial \tau_{yy}}{\partial y}+\dfrac{\partial \tau_{zy}}{\partial z}\\ \dfrac{\partial(\rho w)}{\partial t}+div\left(\rho w\bar{u}\right)=\dfrac{\partial \tau_{xz}}{\partial x}+\dfrac{\partial \tau_{yz}}{\partial y}+\dfrac{\partial \tau_{zz}}{\partial z}-\rho g\end{cases} \tag{4}$$

The governing equations are discretized in time and space, and the discrete governing equations are solved with Finite Volume Method.

3. Numerical Setup

The computational domain is divided into rotating domain of propeller section and van wheel section, solid domains of vane wheel blades, and outer domain. The inlet boundary and outlet boundary are set at distances of 27*D* and 12*D* respectively from the propeller disk. The diameter of the outer domain is 10*D*. The diameter and length of the rotating region of propeller are 2m and 0.52m respectively. The diameter of the rotation domain of vane wheel is 2m, and the length is 0.76m, and the distance between the rotation domain of propeller and the rotation domain of vane wheel is 0.02m. In addition, a cylinder with a diameter and length of 3*D*×3*D* was employed to refine the mesh in the computational domains which surrounds the rotation domains of the propeller and the vane wheel. The layout of computing domains is shown in Figure 1 and table 1.

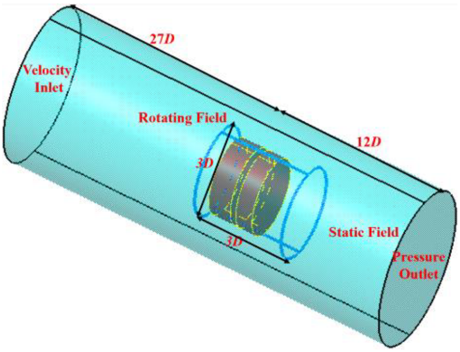

Figure 1. Layout of computational domains.

Table 1. Regions and scale

Region	Scale
Inlet boundary	27*D* from the propeller disk
Outlet boundary	12*D* from the propeller disk
Diameter of the outer domain	10*D*
Diameter of the rotating region of propeller	2m
Length of the rotating region of propeller	0.52m
Diameter of the rotation domain of vane wheel	2m
Length of the rotation domain of vane wheel	0.76m
Distance between the rotation domain of propeller and the rotation domain of vane wheel	0.02m
Diameter of refine domains	3*D*
Length of refine domains	3*D*

The inlet of the stationary domain is set as the velocity inlet. The boundary condition at the outlet of the stationary domain is set as the pressure outlet. The side boundary of the cylindrical stationary domain is set as wall. Interfaces Establish an interface between the stationary domain and two rotating domains.

Polyhedral mesh was used to mesh the computational domains. The polyhedral meshes provide better convergence. Hence, polyhedral meshes are employed in the fluid domains especially for the fluids domain considering morphing. Grids at the leading edge, trailing edge, and the connection of propeller hub are finer than grids in the flow field. The solid domains of vane wheel blades are meshed with structural girds. Overlap mesh method is employed to realize the rotation of vane wheel. The rotation of propeller is realized by sliding mesh method. The mesh details are shown in Figure 2.

Figure 2. Details of mesh.

The solid state physical model is activated in the continuum, the unsteady state, and solid stress models are selected, then the material model and the solid model are defined. The blade of vane wheel in the rotation process has small displacement deformation, its strain relationship follows Hooke's law. At the same time, the material properties of the vane wheel blades are defined as isotropy to maintain the same mechanical properties in all directions. At present study, in addition to conventional nickel-aluminium-bronze materials, new materials are also gradually applied in the field of Marine propulsion. Therefore, the material of vane wheel is set as copper alloy in this paper. Meanwhile, in order to conduct comparative analysis and increase the elastic properties of vane wheel, Young's modulus, density and Poisson's ratio of materials are set as 20GPa, 2100kg/m³ and 0.18, respectively. Other parameters remain unchanged, and the material under this material attribute is denoted as elastic material, as shown in Table 2.

Table 2. Mechanical properties of different materials.

Material	Density (kg/m³)	Elastic modulus (GPa))	Poisson's ratio
Nickel-aluminium-bronze materials	8300	110	0.34
Elastic material	2100	20	0.18

Table 3. Uncertainty analysis of mesh.

	Cells	T	Q	η	ΔT	ΔQ	$\Delta \eta$
Mesh 1	3.56 M	4378.88	764.98	0.2332	-0.91%	-0.30%	-0.64%
Mesh 2	4.54 M	4399.53	768.59	0.2332	-0.45%	0.17%	-0.64%
Mesh 3	5.52 M	4419.28	767.30	0.2347	---	---	---

Uncertainty analysis of mesh is carried out before the numerical study. The results obtained under different mesh are shown in Table 3. Results shown that the hydrodynamic coefficients are convergent as mesh cells increase. The maximum deviation is smaller than 1%. Hence, the Mesh 2 is employed in the numerical study. In

Mesh 2, the size of meshes in the solid domains is 0.01 m. The meshes in the rotation domains and refinement area of outer domain have size of 0.025 m.

4. Results and Discussion

For the vane wheel propulsion system, the thrust coefficient K_{TVR}, torque coefficient K_{QVR}, efficiency η_{VR} of propeller and total thrust coefficient K_T, torque coefficient K_Q, propulsion efficiency η of whole vane wheel propulsion system are calculated with Eq. (5-10):

$$K_{TVR} = \frac{T_{VR}}{\rho n_R^2 D_R^4} \tag{5}$$

$$K_{QVR} = \frac{Q_{VR}}{\rho n_R^2 D_R^5} \tag{6}$$

$$\eta_{VR} = \frac{K_{TVR}}{K_{QVR}} \cdot \frac{J}{2\pi} \tag{7}$$

$$K_T = \frac{T_{VV} + T_{VR}}{\rho n_R^2 D_R^4} \tag{8}$$

$$K_Q = \frac{Q_{VV} + Q_{VR}}{\rho n_R^2 D_R^5} \tag{9}$$

$$\eta = \frac{K_T}{K_Q} \cdot \frac{J}{2\pi} \tag{10}$$

where T_{VR} is thrust of propeller, Q_{VR} is torque of propeller, T_{VV} is the thrust of vane wheel, Q_{VV} is the torque of vane wheel.

The hydrodynamic performance of the nine-blade vane wheel propulsion system under the advance coefficient $J = 0.5$ and 0.8 was carried out, and the comparison was made with the experimental data [6], as shown in Table 4 and figure 3. The deviations between the numerical results and experimental results are below 3% under $J = 0.8$. Hence, the numerical simulation method adopted in this chapter is reliable.

Table 4. Comparison of the results of vane wheel propulsion system and test data.

	Numerical results			Experimental results			Deviations		
J	K_{TR}	$10K_{QR}$	η	K_{TR}	$10K_{QR}$	η	K_{TR}	$10K_{QR}$	η
0.5	0.4854	0.7271	0.5312	0.4596	0.6704	0.5456	-5.60%	-8.45%	2.63%
0.8	0.3060	0.5611	0.6945	0.3076	0.5464	0.7167	0.50%	-2.68%	3.10%

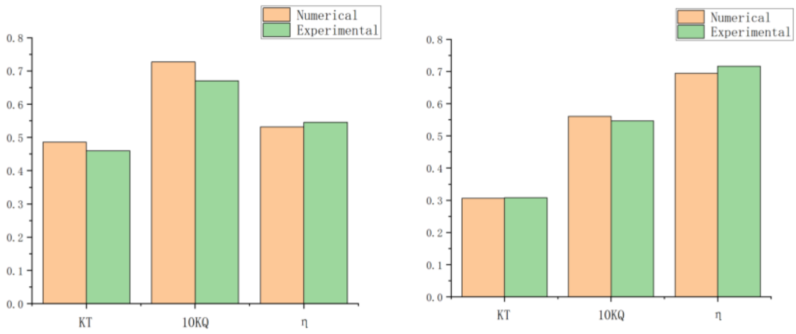

(a) J=0.5 (b) J=0.8

Figure 3. Comparison between numerical results and experimental results.

After the comparison with the experimental values, numerical simulation of the 8-blade vane wheel propulsion system under different advance coefficients was carried out with the above method, as shown in Tables 5-7.

Table 5. Numerical simulation results of the elastic material vane wheel propulsion system.

J	T_{VR}	Q_{VR}	T_{VV}	Q_{VV}	η
0.2	4011.59	768.93	390.29	0	0.2332
0.5	3022.67	638.09	287.35	0	0.5284
0.8	2019.83	493.12	89.42	0	0.6971

Table 6. Numerical simulation results of copper alloy vane wheel propulsion system.

J	T_{VR}	Q_{VR}	T_{VV}	Q_{VV}	η
0.2	4010.00	768.59	389.53	0	0.2332
0.5	3023.59	638.31	287.38	0	0.5284
0.8	2020.00	493.19	89.55	0	0.6971

Table 7. Numerical simulation results of rigid vane wheel propulsion system.

J	T_{VR}	Q_{VR}	T_{VV}	Q_{VV}	η
0.2	3997.21	766.04	390.59	0	0.2334
0.5	3027.48	638.95	288.53	0	0.5286
0.8	2018.03	492.60	90.03	0	0.6974

It can be seen from the Tables 5-7 that the effect of fluid-structure coupling on the hydrodynamic performance is weak. The results show that the hydrodynamic effect on the propulsion system of the vane wheel can be neglected when the fluid-structure interaction is considered. The maximum stress of vane wheel under different advance speed coefficients are compared in Figure 4. It can be seen from the figure that with the increase of the advance coefficient, the stress on the vane wheel blade decreases. That can be attribute to the lighter loading on the vane wheel blade. The stress changes of the two materials have same trends. Under the same advance speed coefficient, the stress of the elastic material paddle is smaller than that of the copper alloy paddle.

The distribution of stress on the vane wheels under different speed coefficients is compared in Figure 5. The unit of stress is MPa. It can be seen from the figure that the stress distribution on the blade of the vane wheel is relatively complex, which relates to the force on the blade of the vane wheel generated by the surrounding wake of upstream propeller and the complex geometric shape of the blade. Under different advance coefficients, the distribution of stress on the vane wheel under different material properties are basically similar, with the maximum stress occurs at about 0.5R of the blade and at the blade root.

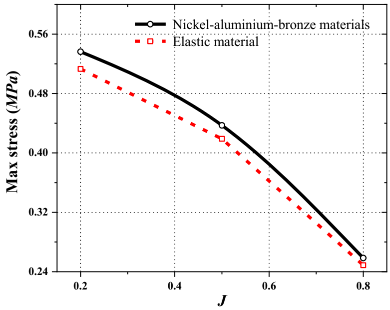

Figure 4. Maximum stress of vane wheel under different speed coefficients.

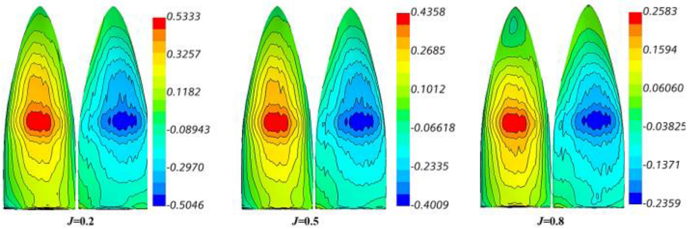

(a) Nickel-aluminium-bronze materials

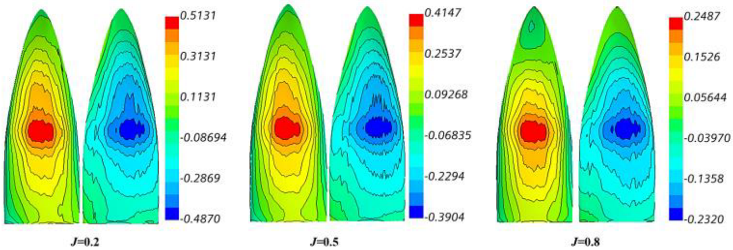

(b) Elastic material

Figure 5. Distribution of stress on the vane wheel.

Figure 6 shows the blade deformation on the vane wheel under different advance coefficients under the two materials. The unit of deformations on the blades is μm. The vane wheel is fixed at the blade root. The deformation increases with the increase of the radial distance of the blade. The maximum deformation occurs at the blade tip which is far away from the blade root. The maximum deformation decreases with the increase of the advance coefficient, which is caused by the decrease of propeller load and wake energy. At the same time, the maximum deformation occurs at the tip of the blade rather than at the maximum stress of the blade can be attribute to the blade thickness decreases gradually with the increase of the blade diameter, so the deformation is easy to occur at blade tip.

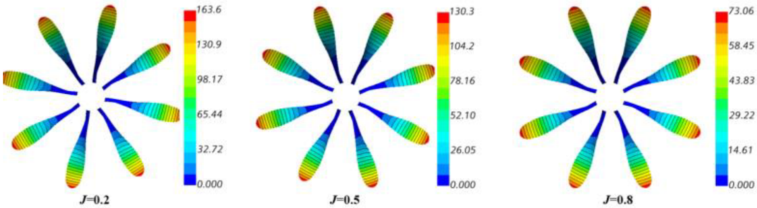

(a) Nickel-aluminium-bronze materials

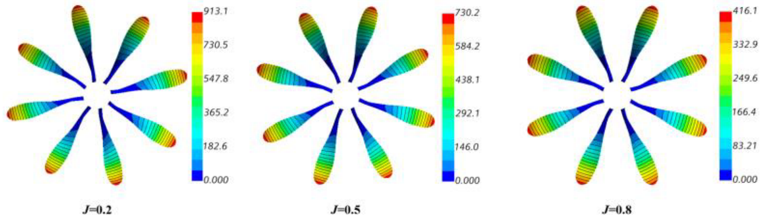

(b) Elastic material

Figure 6. Distribution of deformation on the vane wheel.

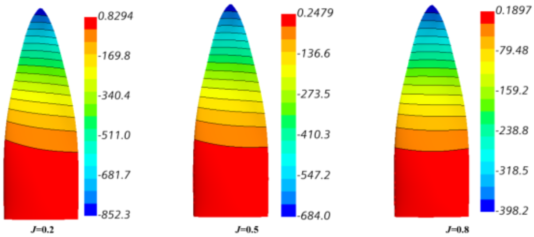

(a) Circumferential deformation

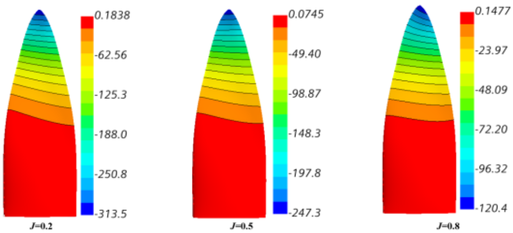

(b) Axial deformation

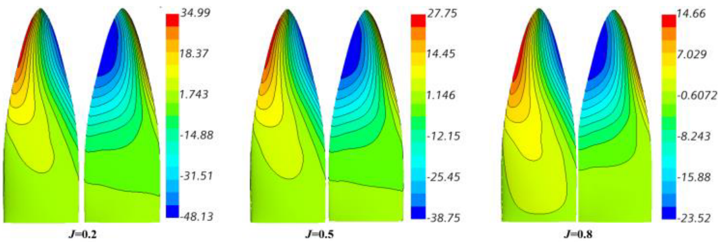

(c) Radial deformation

Figure 7. Deformation at different directions.

Figure 7 shows the circumferential, axial and radial deformation on the single blade of vane wheel at different advance speed coefficients. These results are obtained with elastic material vane wheel. It can be seen from Figure 7(a) and Figure 7(b) that the blade of vane wheel suffers deformations in axial direction and circumferential direction dominantly. That can be attributed to the thrust is mainly caused in axial direction, and the torque is mainly caused in circumferential direction. In Figure 7(c), the deformation at the leading edge is positive, and then gradually decreases towards the trailing edge. The deformation becomes zero near the center line of the blade, and then reaching the maximum at the trailing edge. Due to the trailing edge is thinner than leading edge, radial deformations are more intense at trailing edge.

5. Conclusions

In present study, the deformations on the vane wheel system are numerical studied considering the interaction of fluid structure. The deformation characteristics and hydrodynamic performance prediction of vane wheel are studied. Results show that the difference of hydrodynamic performance between the results considering fluid-structure coupling and rigid propeller is small. The maximum stress of the vane wheel occurs in the middle part of the blade, and diffuses around in a manner similar to concentric circles. Base on the strain analysis results of the vane wheel, the maximum deformation of the vane wheel occurs at the tip of the blade, and the deformation decreases gradually with the increase of the advance coefficient.

References

[1] Grim O. Propeller und Leitrad. 1966.
[2] Grim O. Propeller and Vane Wheel. J Ship Research,1980; 24(04):203-226.
[3] Blaurock J. Propeller Plus Vane Wheel, an unconventional propulsion system. In proceedings: Int Symp on Ship Hydrodynamics and Energy Saving, El Pardo, 6-9 Sept. 1983.
[4] Vanbeek T. Hydrodynamic features of the New QE2 propulsion system. Naval Architect,1987; E219-E222.
[5] Kehr Y Z. Hydrodynamische Analyse des Leitrads, Technische Universität Berlin. 1986.
[6] Chen B Y, Reed A M, Kim K H. A Vane-Wheel Propulsor for a Naval Auxiliary. 1989.
[7] Lee K J, Bae J H, Kim H T, Hoshino T. A performance study on the energy recovering turbine behind a marine propeller. Ocean Eng. 2014; 91:152-158.
[8] Seok W Ch, Suh J C. Algorithm for Performance Analysis of Vane-Wheel using Panel Method. J Society of Naval Architects of Korea, 2013; 50(4):248-254.
[9] Hu J, Zhang W, Sun S, et al. Numerical simulation of interaction between vane wheel and propeller tip vortex. Ships Offshore Struct. 2020; 15(06):620-632.